Journal of Molecular Structure 1051 (2013) 215–220

Contents lists available at ScienceDirect

Journal of Molecular Structure

journal homepage: www.elsevier.com/locate/molstruc

Exploring the effect of chain length of bridging ligands in cobalt(II) coordination polymers based on flexible bis(5,6-dimethylbenzimidazole) ligands: Synthesis, crystal structures, fluorescence and catalytic properties

Li Qin, Yue-Hua Li, Pei-Juan Ma, Guang-Hua Cui *

College of Chemical Engineering, Hebei United University, 46 West Xinhua Road, Tangshan 063009, Hebei, People's Republic of China

HIGHLIGHTS

- Two Co^{II} coordination polymers have been characterized.
- The influences of chain lengths on framework were discussed.
- TG analysis confirms the stability of the coordination polymers.
- Luminescence properties of complexes have been investigated.
- Complexes show higher activity for degradation of methyl orange.

GRAPHICAL ABSTRACT

Two new Co(II) metal–organic coordination polymers have been hydrothermally synthesized using flexible bis(5,6-dimethylbenzimidazole) ligands with varying chain lengths with 5-nitroisophthalic auxiliary ligand. **1** features a 1D looped-like chain consisting of two kinds of macrocycles alternately, and **2** possesses a 4-connected twofold interpenetrating diamond network structure. Moreover, the two compounds as a heterogeneous catalysts present high efficiency for the degradation of methyl orange dye in Fenton-like process.

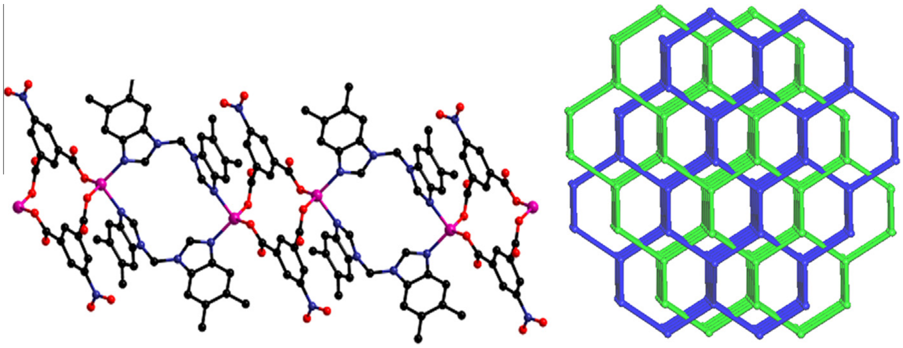

ARTICLE INFO

Article history:
Received 28 May 2013
Received in revised form 25 July 2013
Accepted 9 August 2013
Available online 14 August 2013

Keywords:
Catalytic property
Cobalt(II) coordination polymers

ABSTRACT

Two Co(II) coordination polymers derived from a dicarboxylate and two flexible bis(5,6-dimethylbenzimidazole) ligands with varying chain lengths equipped, namely $[Co(bdmbmm)(nip)]_n$ (**1**) and $[Co_2(bdmbmb)_2(nip)_2 \cdot H_2O]_n$ (**2**) (bdmbmm = 1,1′-bis(5,6-dimethylbenzimidazole)methane, H_2nip = 5-nitroisophthalic acid, bdmbmb = 1,4-bis(5,6-dimethylbenzimidazole)butane), have been synthesized by hydrothermal methods and characterized by elemental analyses, IR spectra, thermogravimetric analysis (TGA), X-ray powder diffraction (XRPD) and single-crystal X-ray diffraction. Complex **1** forms a 1D looped-like chain consisting of two kinds of macrocycles, which is further arranged into a 2D supramolecular layer through face-to-face π–π stacking interactions; whereas complex **2** exhibits a 3D framework

---

Abbreviations: bdmbmm, 1,1′-bis(5,6-dimethylbenzimidazole)methane; bdmbmb, 1,4-bis(5,6-dimethylbenzimidazole)butane; L, 1,3-bis(5,6-dimethylbenzimidazole)propane; H_2nip, 5-nitroisophthalic acid; TGA, thermogravimetric analysis; XRPD, X-ray powder diffraction; MOFs, metal–organic frameworks; AOPs, advance oxidation processes.

* Corresponding author. Tel.: +86 0315 2592169; fax: +86 0315 2592170.

E-mail address: tscghua@126.com (G.-H. Cui).

0022-2860/$ - see front matter
http://dx.doi.org/10.1016/j.molstruc.2013.08.013

Crystal structure
Flexible bis(5,6-dimethylbenzimidazole)
Fluorescence property

with a twofold interpenetrating diamondoid topology. The fluorescence and catalytic properties of the complexes for the degradation of methyl orange by sodium persulfate have been investigated.

1. Introduction

Rational design and construction of cobalt(II) metal–organic coordination polymers has been greatly developed, not only because of their structural diversities, but also owing to their potential applications in gas storage, catalysis, fluorescence, magnetism materials [1–4]. Although coordination bonds still remain at the forefront of crystal engineering strategies, other interactions have received increasing attention over recent years, particularly halogen bonds and hydrogen bonding, π–π interactions [5–7]. Coordination crystalline architectures are intensely influenced by many factors, such as the coordination geometry of metal center, auxiliary ligand, solvent, template, pH value and reaction temperature. Furthermore, the flexibility of the organic ligand also plays a crucial role in determining the final structure of MOFs [8–10]. Therefore, significant interest has arisen in the structural tuning of MOFs through rational selection of bridging ligands. Aromatic polycarboxylate ligands as a kind of O-donor bridging ligands have been extensively used to construct novel metal–organic coordination polymers owing to their remarkable coordination ability and stability [11,12]. Especially, 5-nitroisophthalate with the bending angle of *ca.* 120° between two carboxylate groups may result in extended multi dimensional frameworks [13–15]. In addition, the bis(benzimidazole) ligands bearing alkyl spacers are good choices of N-donor ligand, which can flexibly affect its conformation by means of the $–(CH_2)_n–$ group to meet the requirements of the metal atoms in the assembly process. Among the series of benzimidazole derivatives, the most prominent compound is 5,6-dimethylbenzimidazole, which serves as an axial ligand for cobalt in vitamin B_{12} [16–18]. Bis(5,6-dimethylbenzimidazole) as a bridging ligand participating in construction of coordination polymers can provide more information for us to investigate the influences of methyl substituted derivative of the benzimidazole on the structures and properties of resulting complexes. Moreover, to the best of our knowledge, such metal coordination polymers constructed from bis(5,6-dimethylbenzimidazole) with carboxylate ligands have only been scarcely reported [19,20]. Therefore, the introduction of flexible bis(5,6-dimethylbenzimidazole) ligands into Co(II)-carboxylates system may be an effective synthetic strategy to construct new functional materials.

Azo dyes represent more than 50% of all dyes in common use because of their chemical stability and versatility [21]. Most of them are non-biodegradable, toxic and potentially carcinogenic in nature and at present are abated by some non-destructive processes, such as coagulation, activated carbon adsorption and membrane filtration. Advance oxidation processes (AOPs) are increasingly used as for the reduction of organic contaminants in a variety of wastewaters from different industrial plants [22,23]. Persulfate ($S_2O_8^{2-}$) is one of the strongest oxidants known in aqueous solutions and has the higher potential (E^{ψ} = 2.01 V) than H_2O_2 (E^{ψ} = 1.76 V). It offers some advantages over other oxidants as a solid chemical at ambient temperature with the ease of storage and transport, high stability, high aqueous solubility and relatively low cost [24,25]. Among several AOPs, heterogeneous oxidation is presented as an effective procedure for removing stable organic compounds including dye molecules. Transition metal complexes supported on metal–organic framework are used as potentially active catalysts for the decomposition of $S_2O_8^{2-}$ and the oxidative degradation of organic contaminants and dye.

As our ongoing studies, herein we reported the synthesis and crystal structures of two new coordination polymers $[Co(bdmbmm)(nip)]_n$ (**1**) and $[Co_2(bdmbmb)_2(nip)_2{\cdot}H_2O]_n$ (**2**). Both compounds used as heterogeneous catalysts for the oxidative degradation of methyl orange by persulfate as oxidant have also been investigated in detail.

2. Experimental

2.1. Materials and measurements

All the solvents and reagents for synthesis were obtained from commercial sources and used without further purification. The ligands bdmbmm and bdmbmb were prepared according to literature procedures (see Chart 1) [26]. C, H, and N elemental analyses were performed on a Perkin–Elmer 240C analyzer. FT-IR spectra were recorded on an Avatar 360 (Nicolet) spectrophotometer between 400 and 4000 cm^{-1}, using the KBr pellet method. Thermogravimetric analysis (TGA) was conducted on a Netzsch TG 209 thermal analyzer from room temperature to 800 °C under N_2 with a heating rate of 10 °C/min. The fluorescence spectra were collected with a Hitachi F-7000 spectrophotometer at room temperature. The X-ray powder diffraction (XRPD) patterns were recorded on a Rigaku D/Max-2500 diffractometer at 40 kV, 100 mA for a Cu-target tube and a graphite monochromator. The concentration of methyl orange solution was measured with TU-1901 UV–vis spectrophotometer.

2.2. Preparation of the complexes **1** and **2**

2.2.1. $[Co(bdmbmm)(nip)]_n$ (**1**)

A mixture of $Co(CH_3COO)_2{\cdot}4H_2O$ (0.1 mmol, 24.9 mg), bdmbmm (0.1 mmol, 30.4 mg), H_2nip (0.1 mmol, 21.1 mg) and H_2O (16 mL) was placed in a Teflon-lined stainless steel vessel (25 mL), then the pH value was adjusted to 6.5 by NaOH (0.1 mol/L). The mixture was sealed and heated at 160 °C for 3 days; then, the reaction system was cooled to room temperature at 5 °C/h. Purple block crystals were collected in 20% yield (based on Co). Anal. Calcd. for $C_{27}H_{23}CoN_5O_6$ (Mr = 572.43): C 56.65, H 4.05, N 12.23%. Found: C 56.62, H 4.02, N 12.25%. IR (KBr, cm^{-1}): ν = 3098(w), 3010(w), 1625(s), 1532(m), 1390(m), 1344(m), 1219(w), 1193(w), 733(w), 677(w).

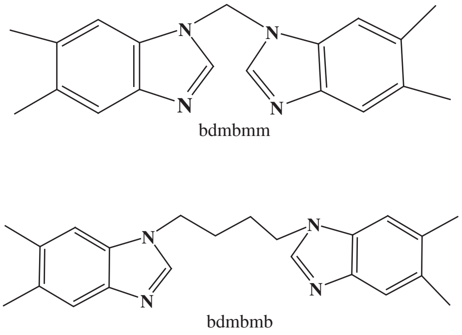

Chart 1. The ligands bdmbmm and bdmbmb.

2.2.2. [$Co_2(bdmbmb)_2(nip)_2 \cdot H_2O]_n$ (**2**)

The synthetic procedure of **2** was similar to the synthesis of **1**, except that bdmbmb (0.1 mmol, 34.6 mg) was used instead of bdmbmm. The purple block crystals of **2** (yield: 35%) were obtained. Anal. Calcd. for $C_{60}H_{60}Co_2N_{10}O_{13}$ (Mr = 1247.06): C 57.79, H 4.85, N 11.23%. Found: C 57.76, H 4.88, N 11.25%. IR (KBr, cm^{-1}): ν = 3407(vs), 2938(w), 1620(s), 1561(m), 1383(w), 1348(w), 1154(w), 1084(w), 733(w), 623(w).

2.3. Catalytic experimental procedures

The catalytic experiments were performed in 250-mL round-bottom flask. Reaction solutions were obtained by adding the solid catalysts **1** (or **2**) into aqueous methyl orange solution and the initial pH of the reaction solution was adjusted with H_2SO_4 (0.1 mol/L) solution reaching to 3. Then the reaction was initiated by adding sodium persulfate (0.2 g/L) into the prepared reaction solutions with a total volume of 150 mL. At the given time intervals, the samples were filtered through a 0.45 μm membrane filter before measurement. All experiments were carried out at a temperature of 30 °C.

The efficiency of the proposed process was evaluated by monitoring methyl orange degradation by measuring absorbance at 506 nm using a double beam UV/vis spectrophotometer. Therefore, the concentration of the methyl orange in the reaction mixture at different reaction times was determined by measuring the absorption intensity at λ_{max} = 506 nm and from a calibration curve. Prior to the measurement, a calibration curve was obtained by using the standard methyl orange solution with known concentrations. Because the reaction continued after sampling, the measurement of absorbance of reaction solution was done within 1 min.

The degradation efficiency of methyl orange was defined as follows: [27]

$$\text{Degradation efficiency} = \frac{(C_0 - C_t)}{C_0} \times 100\% \qquad (1)$$

where C_0 (mg/L) is the initial concentration of methyl orange, and C_t (mg/L) is the concentration of methyl orange at reaction time, t (min).

2.4. X-ray crystallography

Crystallographic data for **1** and **2** were collected on a Bruker Smart 1000 CCD diffractometer using graphite-monochromated Mo Kα radiation (λ = 0.71073 Å) at room temperature with ω-scan mode. A semi-empirical absorption correction was applied using SADABS program [28]. The structures were solved by direct methods and refined on F^2 by full-matrix least-squares using SHELXTL-97 [29]. All non-hydrogen atoms were refined anisotropically. In the structure of **2**, the one water molecules is disordered. This structure was refined by the SQUEEZE routine of the PLATON program [30]. The crystallographic data for **1** and **2** are listed in Table 1, and selected lengths and angles parameters for **1** and **2** are presented in Table S1, respectively.

3. Results and discussion

3.1. Crystal structures of **1**

Compound **1** crystallizes in the monoclinic space group $P\bar{1}$. The results of crystallographic analysis reveal that the asymmetric unit of **1** consists of one Co(II) atom, one bdmbmm ligand and one nip^{2-} ligand. As shown in Fig. 1a, each Co(II) atom is four-coordinated by two carboxylate oxygen atoms from two different nip^{2-} anions and two nitrogen atoms from two bdmbmm ligands, showing a tetrahedral geometry {CoN_2O_2}. The Co–N bond distances are 2.027(3) and 2.062(3) Å, and the Co–O bond lengths are 1.965(2) and 1.978(2) Å, both of which are in the normal range [31,32].

Table 1
Crystal and refinement data for complexes **1** and **2**.

	1	**2**
Empirical formula	$C_{27}H_{23}CoN_5O_6$	$C_{60}H_{60}Co_2N_{10}O_{13}$
Formula weight	572.43	1247.06
Crystal system	Triclinic	Monoclinic
Space group	$P\bar{1}$	$C2/c$
a (Å)	7.1538(8)	16.1902(18)
b (Å)	12.2333(13)	23.799(3)
c (Å)	15.2989(17)	16.0948(18)
α (°)	69.8510(10)	
β (°)	83.0780(10)	112.444(2)
γ (°)	88.825(2)	
V ($Å^3$)	1247.5(2)	5731.7(11)
Z	2	4
D_{calc} (g/m^3)	1.524	1.424
μ (mm^{-1})	0.742	0.651
$F(000)$	590	2552
Crystal size (mm)	0.15 × 0.12 × 0.11	0.22 × 0.16 × 0.11
Total reflections	6400	14,602
Unique reflections	4346	5051
R_{int}	0.0246	0.0690
GOF	1.074	0.971
R_1 ($I > 2\sigma(I)$)	0.0438	0.0638
wR_2 ($I > 2\sigma(I)$)	0.0985	0.1492
$\Delta\rho$max ($eÅ^{-3}$)	0.295	0.906
$\Delta\rho$min ($eÅ^{-3}$)	−0.292	−0.469

$R_1 = \Sigma||F_o|-|F_c||/\Sigma|F_o|$; $wR_2 = \Sigma\,[wF_o^2 - F_c^{22}]/\Sigma\,[wF_o^{22}]^{1/2}$.

1 Displays a looped-like chain containing two kinds of macrocycles alternately (Fig. 1b). Two 5-nitroisophthalates adopting bis (monodentate) coordination mode bridge adjacent Co atoms to form a 16-membered macrocycle [$Co_2(nip)_2$] with the Co1···Co1#1 distance of 6.5179(9) Å. Another kind of macrocycle [Co_2(bdmbmm)$_2]^{4+}$ is constructed by two bdmbmm ligands, showing bis-monodentate mode coordinating to the center atoms with the Co1···Co1#2 separation of 8.3793(9) Å (symmetry code #1: $-x+1$, $-y+1$, $-z$; #2: $-x+2$, $-y$, $-z$). Each bdmbmm ligand in **1** adpots *cis*-configuration and the dihedral angle between the mean-planes of the two benzimidazole rings is 67.577°. Furthermore, the adjacent 1D layers are extended into a 2D supramolecular framework by the π–π stacking interactions with the center-to-center separations of 3.504 Å and 3.6045 Å between neighboring imidazole rings and benzene rings, and neighboring benzene rings and benzene rings from benzimidazoles, respectively (Fig. 1c). Besides that, weak intermolecular hydrogen bonding interactions also exist with a H(11)···O(2) distance of 2.25 Å and the angle of 150° [C(11)–H(11)···O(2)] that further stabilize the crystal packing.

3.2. Crystal structures of **2**

As compared to complex **1**, the bdmbmm coligand is replaced by bdmbmb, and the resulting structure is a twofold interpenetrating 3D diamond framework. Single-crystal X-ray diffraction analysis reveals that **2** crystallizes in the monoclinic space group $C2/c$, and the asymmetric unit contains one Co(II) atom, one bdmbmb ligand, one nip dianion and one guest water molecule. The coordination environment around Co(II) is shown in Fig. 2a. Each Co(II) atom sits in a distorted tetrahedron geometry defined by two nitrogen atoms [Co1–N3 = 2.011(4) Å and Co1–N1 = 2.033(4) Å] of two bdmbmb ligands and two oxygen atoms [Co1–O4#1 = 1.954(4) Å and Co1–O2 = 1.964(3) Å] (symmetry code #1: $x+1/2$, $-y+1/2$, $z+1/2$) from two separated nip^{2-} anions. The Co–O/N bond lengths are all consistent with corresponding bond lengths found in the literature [33].

The two carboxylic groups of nip^{2-} take a uniform coordination mode, all in a $\mu_2 - \eta^1{:}\eta^1$ fashion. Co(II) atoms are connected by nip^{2-}

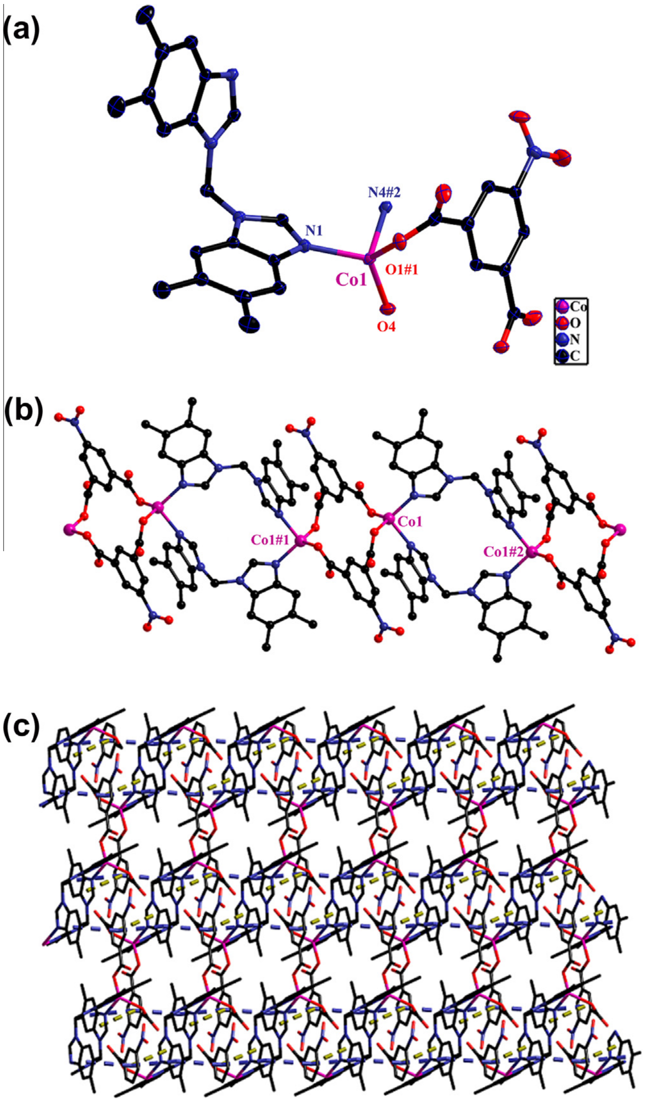

Fig. 1. (a) The coordination environment of Co(II) atom in complex **1** with 30% thermal ellipsoids. Hydrogen atoms and the free water molecule are omitted for clarity. (b) The 1D looped-like chain for **1**. (c) 2D supramolecular networks by π–π stacking interactions (symmetry code #1: $-x + 1$, $-y + 1$, $-z$; #2: $-x + 2$, $-y$, $-z$).

anions to form a 1D chain. Furthermore, the bdmbmb ligands crosslinking these 1D chains along the two directions, finally resulting in a 3D framework (Fig. 2b). Analysis of network topology provides a convenient tool in designing and understanding the complicated crystal structures of coordination polymers. Such structures can usually be reduced to simple topological networks with different connectivity of the components. Thus, the 3D structure of **2** can be reduced as a classical diamond net (dia) by TOPOS 4.0 program [34]. Each Co center bridges four other Co atoms, viewed as 4-connected nodes in tetrahedral sphere and nip^{2-} and bdmbmb ligands as linkers (Fig. 2c). Notably, the large voids formed by a single 3D network allow incorporation of the other identical network. Therefore, the overall structure of **2** has two identical 3D nets, which interpenetrate each other to generate a twofold interpenetrating dia architecture belonging to class IIa (Fig. 2d).

3.3. Effect of the spacer length of flexible bis(5,6-dimethylbenzimidazole) ligands

It is well known that the spacer length of the flexible organic ligands play an important role in determining their final structures

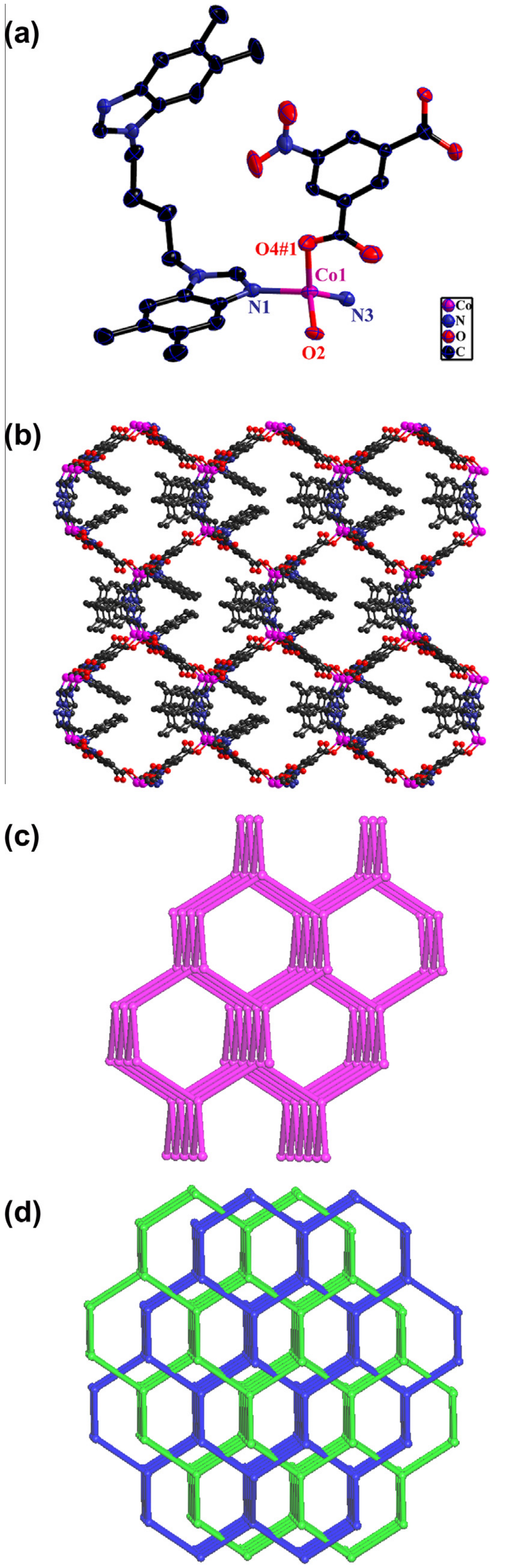

Fig. 2. (a) The coordination environment of Co(II) atom in complex **2** with 30% thermal ellipsoids. Hydrogen atoms and the free water molecule are omitted for clarity (symmetry code #1: $x + 1/2$, $-y + 1/2$, $z + 1/2$). (b) The 3D framework of **2**. (c) Schematic illustrating the 3D diamond topology in **2**. (d) The twofold interpenetrating diamond architecture of **2**.

of the complexes. Compound **3**, named $[Co(L)(nip)]_n$ (L = 1,3-bis(5,6-dimethylbenzimidazole)propane) has been previously synthesized and its structure published [31]. By varying the $–(CH_2)_n–$ length (n = 1, 4, 3) of flexible bis(5,6-dimethylbenzimidazole) ligands, the three related Co(II) compounds with different structures (1D, 3D and 2D) were successfully obtained under the similar synthetic conditions. In complexes **1**–**3**, all of these three flexible N-containing ligands present a μ_2-bridging coordination mode, but $–(CH_2)_n–$ (n = 1, 4, 3) spacers exhibit different bending and rotating ability, which lead to generating different non-bonding Co···Co distances (8.38 Å for **1**, 10.62 Å for **2**, 9.83 Å for **3**) and the different dihedral angles (67.58° in **1**, 65.63° in **2**, 73.89° in **3**) between two benzimidazole rings with the entire bis(5,6-dimethylbenzimidazole) ligand. Although the three Co(II) complexes contain the same dicarboxylate (nip^{2-}) secondary ligand, the coordination mode of nip^{2-} anions is different (a $\mu_2–\eta^1:\eta^1$ mode in compounds **1** and **2**, a $\mu_3–\eta^1:\eta^2$ mode in compound **3**). Thus, Co(II) ions are bridged by nip^{2-} ligands and different flexible bis(5,6-dimethylbenzimidazole) ligands to generate 1D looped-like chain for **1**, 3D twofold interpenetrating diamond architecture for **2**, 2D (4,4) layer for **3**. The 2D supermolecular framework for compound **1** is formed by $\pi–\pi$ stacking interactions due to the existence of aromatic rings from organic ligands. And hydrogen bonds or $\pi–\pi$ stacking interactions in **2** and **3** are to further stabilize the crystal structures.

3.4. IR spectra

The main features of IR spectra for complexes **1** and **2** concerned the carboxylate groups of nip^{2-} ligand and the bdmbmm or bdmbmb ligand. No strong absorption peaks around 1700 cm^{-1} for –COOH are observed, which implies that carboxyl groups of organic moieties in the title complexes are completely deprotonated [35,36]. The strong peaks at 1625 and 1390 cm^{-1} for **1**, and 1620 and 1383 cm^{-1} for **2** may be attributed to the asymmetric and symmetric vibrations of carboxylate groups. The presence of the expected characteristic bands at 1532, 1193 and 733 cm^{-1} for **1**, and 1561, 1084 and 733 cm^{-1} for **2**, suggest the $\nu_{C–N}$ stretching of the benzimidazole ring of the bdmbmm or bdmbmb ligand. For **2**, it shows strong and broad peak around 3407 cm^{-1} relating to the O–H stretching vibration modes of water molecules.

3.5. X-ray Powder diffraction (XRPD) and thermogravimetric analysis (TGA)

To confirm the phase purity of compounds **1** and **2**, the as-synthesized samples were characterized by XRPD at room temperature, as shown in Fig. S1. Although the experimental patterns have a few un-indexed diffraction lines and some are slightly broadened in comparison with those simulated from the single-crystal models (perhaps they come from the impurity attached to the surface of crystal samples), it still can be well considered that the bulk synthesized materials and the crystals used for diffraction are homogeneous.

To characterize the compounds more fully in terms of thermal stability, the thermal behaviors of **1** and **2** were examined by TGA (Fig. S2). The experiments were performed on samples consisting of numerous single crystals under an N_2 atmosphere with a heating rate of 10 °C/h. For complex **1**, two weight loss steps were observed. The continuous one from 270 to 330 °C is attributed to the loss of the nip^{2-} ligand. The weight loss is about 33.08% in correspondence with the calculated value of 33.74%. The sharp weight loss is observed in the range 408–663 °C, corresponding to the decomposition of bdmbmm ligands (53.04%, calculated value of 53.11%). The remaining weight (13.88%) corresponds to the percentage (13.09%) of Co and O components in CoO, indicating that is the final product. For **2**, the first weight loss corresponding to the release of lattice water molecules is observed in the temperature range of 65 to 102 °C (obsd 1.69%, calcd 1.44%), and the departure of organic components occurs from 314 °C.

To check the final products of thermal analysis, XRPD was carried out at room temperature (Fig. S3). The experimental XRPD patterns perfectly match the simulated patterns based on the single crystal X-ray data with CoO.

3.6. Fluorescence properties

Coordination frameworks with metal centers and N-donor ligands linkers are promising candidates for photoactive materials with potential applications in chemical sensors, photochemistry and electroluminescent display [37,38]. Thus, the solid state fluorescence properties of Co(II) compounds **1** and **2**, together with the free bdmbmm and bdmbmb ligands were investigated at room temperature (Fig. 3). The free ligands bdmbmm and bdmbmb exhibit the emission peaks at 318 nm and 370 nm with the excitations at 313 nm and 270 nm, respectively, which can probably be assigned to the $\pi \rightarrow \pi^*$ transitions [39]. The fluorescence peaks at about 418 nm for **1** and 423 nm for **2** are found in the emission spectra when they are excited at 274 nm and 325 nm, respectively. As previously reported, the solid aromatic carboxylate ligand H_2nip are nearly nonfluorescent in the range 400–600 nm at ambient

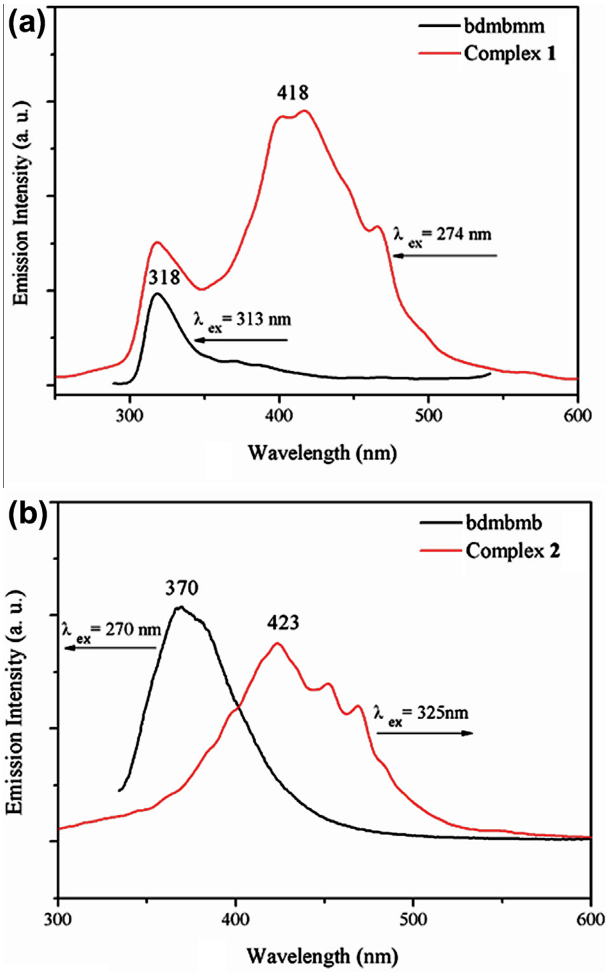

Fig. 3. (a) Solid-state photoluminescence spectra of complex **1** and free ligand bdmbmm. (b) Solid-state photoluminescence spectra of complex **2** and free ligand bdmbmb.

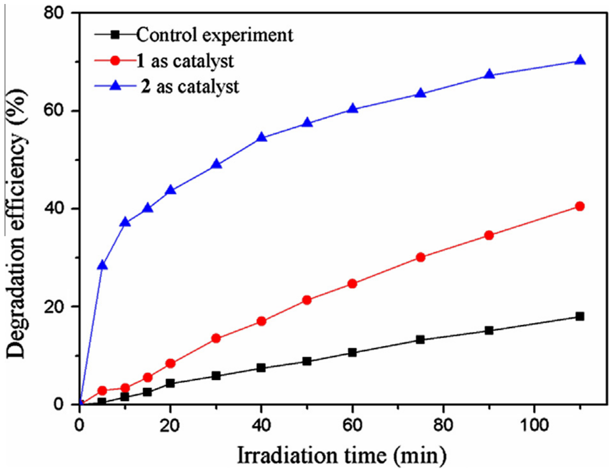

Fig. 4. Degradation of methyl orange in persulfate systems.

temperature [40]. For complexes **1** and **2**, it is clear that an obvious red-shifted (100 nm for **1**, 53 nm for **2**) emission band has been observed compared with the free bdmbmm and bdmbmb ligands. Therefore, the fluorescence behaviors of **1** and **2** can be tentatively ascribed to the ligand-to-metal charge-transfer, which is similar to the reported metal complexes with N-donor ligands [40]. The varying degrees of red shift may be attributed to different coordination environments of N-containing ligands and the different structures caused by different organic bi-carboxylates in this work [41].

3.7. Catalytic properties

In the study, methyl orange was selected as a model compound of organic pollutant and the degradation using the heterogeneous catalysts complexes **1** or **2** in the presence of persulfate are depicted in Fig. 4. When the research was conducted at control experiment (no catalyst), only 17.9% of the azo dye is decomposed after 110 min, indicating that methyl orange cannot be effectively oxidized by persulfate solely. However, when the using complex **1** (or **2**) as catalyst, a reaction quickly takes place leading to a color removal of the methyl orange dye. Degradation efficiencies can reach 40.5% for complex **1**, 70.1% for complex **2** after 110 min under the same condition. The complexes can catalyze persulfate to produce more strongly oxidizing sulfate radicals ($SO_4^{\cdot -}$) [42] and further increase the efficiency of the pollutant degradation significantly. The difference catalytic performances of the two complexes may be due to the distinct coordination environments around the metal centers [32]. Based on the experimental findings, a reaction mechanism can be suggested as the follows [42]:

$$S_2O_8^{2-} + Co^{II} - MOF \rightarrow Co^{III} - MOF + SO_4^{2-} + SO_4^{\cdot -} \quad (2)$$

$$SO_4^{\cdot -} + Co^{II} - MOF \rightarrow Co^{III} - MOF + SO_4^{2-} \quad (3)$$

$$\text{Dye} + SO_4^{\cdot -} \rightarrow \text{oxidation products} \quad (4)$$

4. Conclusion

Two Co(II) coordination polymers based on bis(5,6-dimethylbenzimidazol) and H_2nip ligands have been synthesized hydrothermally. The structural analysis demonstrates that chain lengths of the bridging ligands can greatly affect the resulting coordination and supramolecular architectures. Both complexes, especially **2**, show high catalytic activities in the Fenton-like decomposition of methyl orange.

Appendix A. Supplementary material

CCDC 917955 and 917953 contain the supplementary crystallographic data for the complexes **1** and **2**. These data can be obtained free of charge *via* http://www.ccdc.cam.ac.uk/conts/retrieving.html, or from the Cambridge Crystallographic Data Centre, 12 Union Road, Cambridge CB21EZ, UK; fax: +44 1223 336 033; or e-mail: deposit@ccdc.cam.ac.uk. Supplementary data associated with this article can be found, in the online version, at http://dx.doi.org/10.1016/j.molstruc.2013.08.013.

References

[1] G.C. Liu, J.J. Huang, J.W. Zhang, X.L. Wang, H.Y. Lin, Trans. Met. Chem. 38 (2013) 359–365.
[2] S.R. Batten, R. Robson, Angew. Chem. Int. Ed. 37 (1998) 1460–1494.
[3] Y.Y. Liu, B. Liu, J. Yang, J.F. Ma, Polyhedron 56 (2013) 96–101.
[4] J.C. Geng, L. Qin, X. Du, S.L. Xiao, G.H. Cui, Z. Anorg, Allg. Chem. 638 (2012) 1233–1238.
[5] D.K. Kumar, Inorg. Chim. Acta 362 (2009) 1767–1771.
[6] T.J. Burchell, D.J. Eisler, R.J. Puddephatt, Inorg. Chem. 43 (2004) 5550–5557.
[7] J.Q. Chen, Y.P. Cai, H.C. Fang, Z.Y. Zhou, X.L. Zhan, G. Zhao, Z. Zhang, Cryst. Growth Des. 9 (2009) 1605–1613.
[8] Y.Y. Liu, Y.Y. Jiang, J. Yang, Y.Y. Liu, J.F. Ma, CrystEngComm 13 (2011) 6118–6129.
[9] S.L. Xiao, X. Du, L. Qin, C.H. He, G.H. Cui, J. Inorg. Organomet. Polym. 22 (2012) 1384–1390.
[10] L. Qin, S.L. Xiao, P.J. Ma, G.H. Cui , Trans. Met. Chem. 38 (2013) 627–633.
[11] R. Sun, Y.Z. Li, J.F. Bai, Y. Pan, Cryst. Growth Des. 7 (2007) 890–894.
[12] X. Zhu, P.P. Sun, J.G. Ding, B.L. Li, H.Y. Li, Cryst. Growth Des. 12 (2012) 3992–3997.
[13] A. Heba, M. Brian, K. Victor, J.Z. Michael, J. Am. Chem. Soc. 124 (2002) 9990–9991.
[14] M. Du, Z.H. Zhang, Y.P. You, X.J. Zhao, CrystEngComm 10 (2008) 306–321.
[15] X.Y. Lu, J.W. Ye, W. Li, W.T. Gong, L.J. Yang, Y. Lin, G.L. Ning, CrystEngComm 14 (2012) 1337–1344.
[16] S.S. Marwaha, R.P. Sethi, J.F. Kennedy, Enzyme Microbiol. Technol. 5 (1983) 361–364.
[17] S.L. Xiao, L. Qin, C.H. He, X. Du, G.H. Cui, J. Inorg. Organomet. Polym. 23 (2013) 771–778.
[18] J.C. Geng, C.H. Jiao, J.M. Hao, G.H. Cui, Z. Naturforsch. 67b (2012) 791–798.
[19] X.L. Wang, S. Yang, G.C. Liu, J.X. Zhang, H.Y. Lin, A.X. Tian, Inorg. Chim. Acta 375 (2011) 70–76.
[20] C.H. Jiao, C.H. He, J.C. Geng, G.H. Cui, J. Coord. Chem. 65 (2012) 2852–2861.
[21] X.R. Xu, X.Z. Li, Sep. Purif. Technol. 72 (2010) 105–111.
[22] W.H. Glaze, J.W. Kang, D.H. Chapin, Ozone Sci. Eng. 9 (1987) 335–352.
[23] T.K. Lau, W. Chu, N.J.D. Graham, Environ. Sci. Technol. 41 (2007) 613–619.
[24] L. Qin, J. Zheng, S.L. Xiao, X.H. Zheng, G.H. Cui, Inorg. Chem. Commun. 34 (2013) 71–74.
[25] D. Zhao, X.Y. Liao, X.l. Yan, S.G. Hulingc, T. Chaia, H. Tao, J. Hazard. Mater. 2254–2255 (2013) 228–235.
[26] L.L. Li, H.X. Li, Z.G. Ren, D. Liu, Y. Chen, Y. Zhang, J.P. Lang, Dalton Trans. 40 (2009) 8567–8573.
[27] B.H. Hameed, T.W. Lee, J. Hazard. Mater. 164 (2009) 468–472.
[28] G.M. Sheldrick, SADABS (version 2.03), Program for Empirical Absorption Correction of Area Detector Data, University of Göttingen, Göttingen, Germany, 1996.
[29] G.M. Sheldrick, Acta Crystallogr. Sect., A 64 (2008) 112–122.
[30] A.L. Spek, Acta Cryst. D65 (2009) 148–155.
[31] G.C. Liu, S. Yang, X.L. Wang, H.Y. Lin, A.X. Tian, J.W. Zhang, Russ. J. Coord. Chem. 38 (2012) 55–60.
[32] J.C. Geng, L.W. Liu, S.L. Xiao, G.H. Cui, Trans. Met. Chem. 38 (2013) 143–148.
[33] S. Hayami, K. Murata, D. Urakami, Y. Kojima, M. Akita, K. Inoue, Chem. Commun. (2008) 6510–6512.
[34] V.A. Blatov, Struct. Chem. 23 (2012) 955–963.
[35] X.J. Gu, D.F. Xue, Cryst. Growth Des. 6 (2006) 2551–2557.
[36] L.J. Bellamy, The Infrared Spectra of Complex Molecules, Wiley, New York, 1958.
[37] Y.Q. Lan, H.L. Jiang, S.L. Li, Q. Xu, Inorg. Chem. 51 (2012) 7484–7491.
[38] D. Niu, J. Yang, J. Guo, W.Q. Kan, S.Y. Song, P. Du, J.F. Ma, Cryst. Growth Des. 12 (2012) 2397–2410.
[39] H.Y. Bai, J. Yang, B. Liu, J.F. Ma, W.Q. Kan, Y.Y. Liu, Y.Y. Liu, CrystEngComm 13 (2011) 5877–5884.
[40] H. Ren, T.Y. Song, J.N. Xu, S.B. Jing, Y. Yu, P. Zhang, L.R. Zhang, Cryst. Growth Des. 9 (2009) 105–112.
[41] X.L. Wang, J.X. Zhang, G.C. Liu, H.Y. Lin, Y.Q. Chen, Z.H. Kang, Inorg. Chim. Acta 368 (2011) 207–215.
[42] M.C. Yeber, L. Díaz, J. Fernández, J. Photochem. Photobiol. A: Chem. 215 (2010) 90–95.